Supporting Information

Luminescence of Mn^{2+} ion in non-O_h and T_d coordination environments: the missing case of square pyramid

Alexander V. Artem'ev,*[a,b] Maria P. Davydova,[a] Alexey S. Berezin,[a,b] Valery K. Brel,[c] Vasilii P. Morgalyuk,[c] Irina Yu. Bagryanskaya,[b,d] Denis G. Samsonenko[a,b]

[a] Nikolaev Institute of Inorganic Chemistry, Siberian Branch of Russian Academy of Sciences, 3, Acad. Lavrentiev Ave., Novosibirsk 630090, Russian Federation
[b] Novosibirsk State University, 2, Pirogova Str., Novosibirsk 630090, Russian Federation
[c] A. N. Nesmeyanov Institute of Organoelement Compounds, Russian Academy of Sciences, 28, Vavilova Str., Moscow, 119991, Russian Federation
[d] N. N. Vorozhtsov Novosibirsk Institute of Organic Chemistry, Siberian Branch of Russian Academy of Sciences, 9, Acad. Lavrentiev Ave., Novosibirsk 630090, Russian Federation Center for Optical and Laser Materials Research, Saint Petersburg State University, Ulianovskaya, 5, Saint Petersburg 198504, Russian Federation

*Author for correspondence: chemisufarm@yandex.ru (Alexander V. Artem'ev)

Table of Contents

§1. X-Ray crystallography

Single crystals of **1**–**3** were grown by vapor diffusion of diethyl ether into an acetonitrile solution at room temperature for several days. Diffraction data for single-crystals of **1** and **2** were collected on a Bruker Kappa Apex II CCD diffractometer using φ,ω-scans of narrow (0.5°) frames with MoKα radiation (λ = 0.71073 Å) and a graphite monochromator. The data for crystals of **3** were obtained on an automated Agilent Xcalibur diffractometer equipped with an area AtlasS2 detector (graphite monochromator, λ(MoKα) = 0.71073 Å, ω-scans). Integration, absorption correction, and determination of unit cell parameters were performed using the CrysAlisPro program package.[1] The structures were solved by dual space algorithm (SHELXT[2]) and refined by the full-matrix least squares technique (SHELXL[3]) in the anisotropic approximation (except hydrogen atoms). Positions of hydrogen atoms of organic ligands were calculated geometrically and refined in the riding model. For the structure **2**, solvate molecules (MeCN and H_2O) are highly disordered and cannot be refined as a set of discrete atoms. We employed PLATON/SQUEEZE procedure[4] to calculate the contribution to the diffraction from the solvent region and thereby produced a set of solvent-free diffraction intensities. Total composition of the structure **2** was calculated with the agreement of SQUEEZE procedure (196 e in 911 Å^3). This corresponds to the formula **2**·4MeCN·H_2O.

The crystallographic data and details of the structure refinements are summarized in Table S1. CCDC 1921850, 1921851 and 1921523 contain the supplementary crystallographic data for this paper. These data can be obtained free of charge from The Cambridge Crystallographic Data Center at http://www.ccdc.cam.ac.uk/data_request/cif.

[1] CrysAlisPro 1.171.38.46, Rigaku Oxford Diffraction, 2015.
[2] G.M. Sheldrick *Acta Crystallogr*., 2015, **A71**, 3–8.
[3] G.M. Sheldrick, *Acta Crystallogr*., 2015, **C71**, 3–8.
[4] A.L. Spek, Acta Crystallogr., 2015, **C71**, 9–18.

Table S1. Crystal data and structure refinement for **1–3**.

	1	2	3
CCDC	1921851	1921850	1921523
Chemical formula	$C_{54}H_{54}Br_2MnN_2O_4P_4$	$C_{143}H_{149}Cl_6Mn_3N_9O_{11}P_{10}$	$C_{56}H_{57}ClIMnN_3O_4P_4$
M_r (g·mol^{-1})	1133.66	2856.92	1177.21
Crystal system, space group	Triclinic, $P1$	Triclinic, $P1$	Monoclinic, $P2_1$
Temperature (K)	296	296	130
a, b, c (Å)	14.1360(13), 14.4046(10), 14.9017(13)	17.7199(7), 20.7944(9), 21.1999(9)	11.2811(7), 17.8990(9), 14.2259(8)
α, β, γ (°)	63.853(3), 86.986(4), 84.516(4)	88.311(2), 85.202(2), 68.366(2)	109.443(6)
V (Å^3)	2711.2(4)	7235.9(5)	2708.7(3)
Z	2	2	2
μ (mm^{-1})	1.88	0.54	1.03
Crystal size (mm)	0.40 × 0.40 × 0.20	0.60 × 0.30 × 0.10	0.40 × 0.12 × 0.07
No. of measured, independent and observed [$I > 2\,\sigma(I)$] reflections	40988, 9502, 5727	132295, 26486, 14009	13160, 9477, 9090
R_{int}	0.058	0.076	0.016
$(\sin\theta/\lambda)_{max}$ (Å^{-1})	0.595	0.602	0.681
$R[F^2 > 2\sigma(F^2)]$, $wR(F^2)$, S	0.078, 0.238, 1.06	0.076, 0.240, 1.06	0.027, 0.064, 1.04
No. of reflections	9502	26486	9477
No. of parameters	607	1527	637
$\Delta\rho_{max}, \Delta\rho_{min}, e$ Å^3	1.42, −0.54	1.36, −1.01	0.53, −0.56
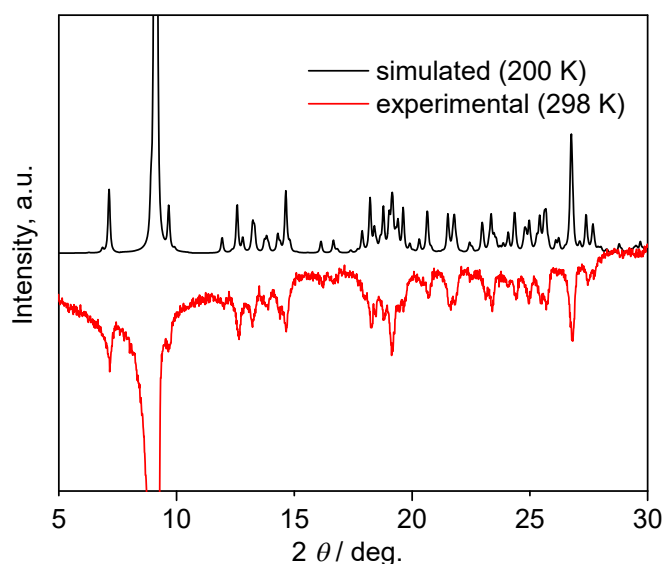
Figure S1. Experimental and simulated XRPD patterns for "as-synthesized" sample of **1**.
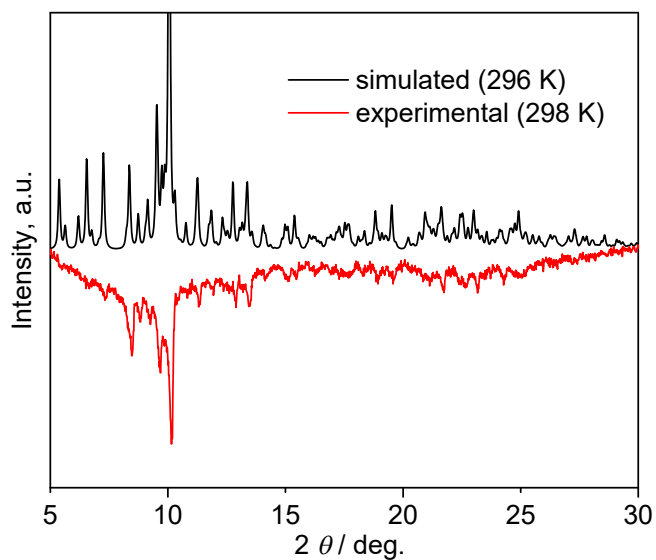
Figure S2. Experimental and simulated XRPD patterns for "as-synthesized" sample of **2**.
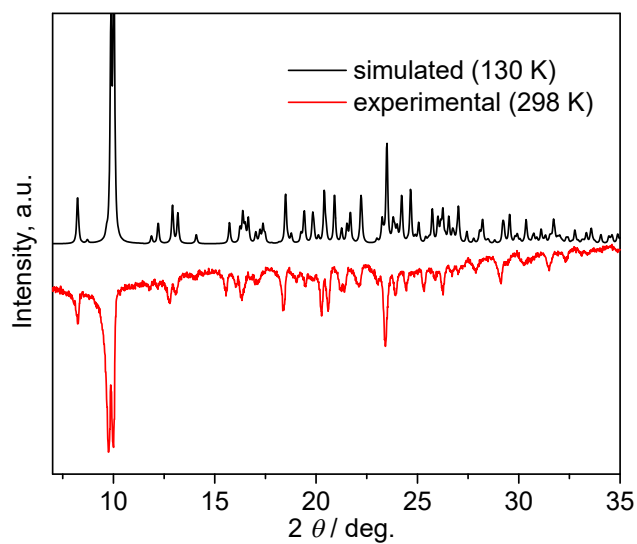
Figure S3. Experimental and simulated XRPD patterns for "as-synthesized" sample of **3**.

§2. TG, DTG and c-DTA curves
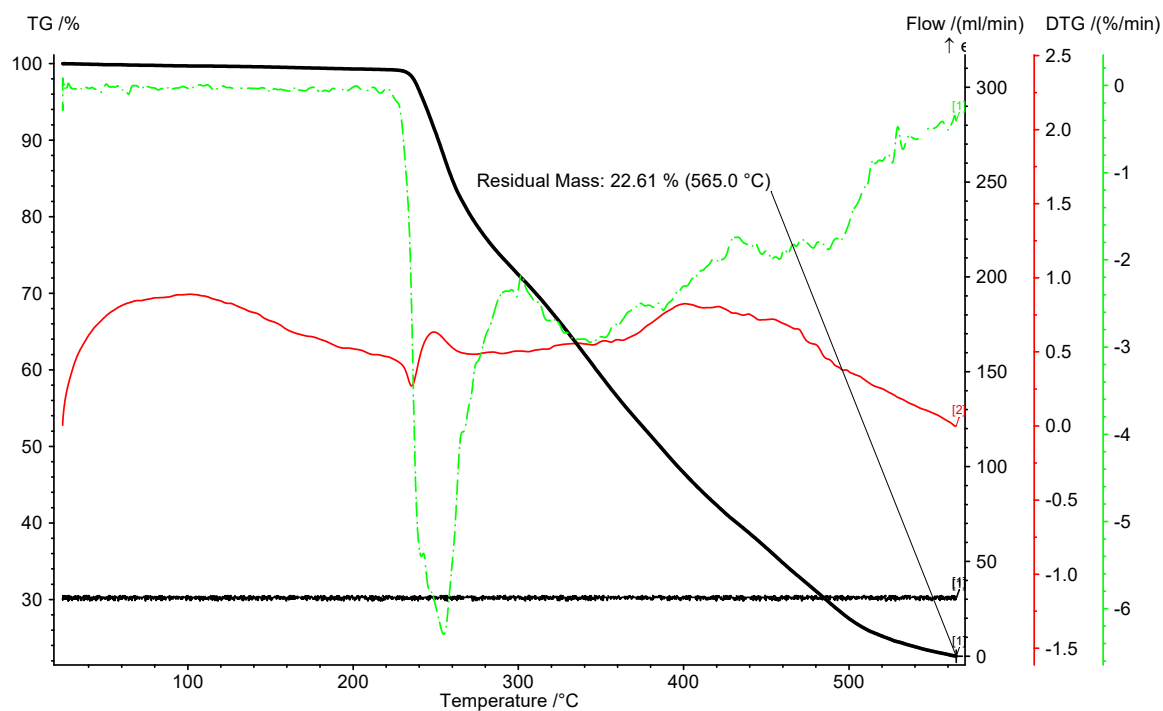
Figure S4. The TGA, DTA & DTG curves for complex **1**.
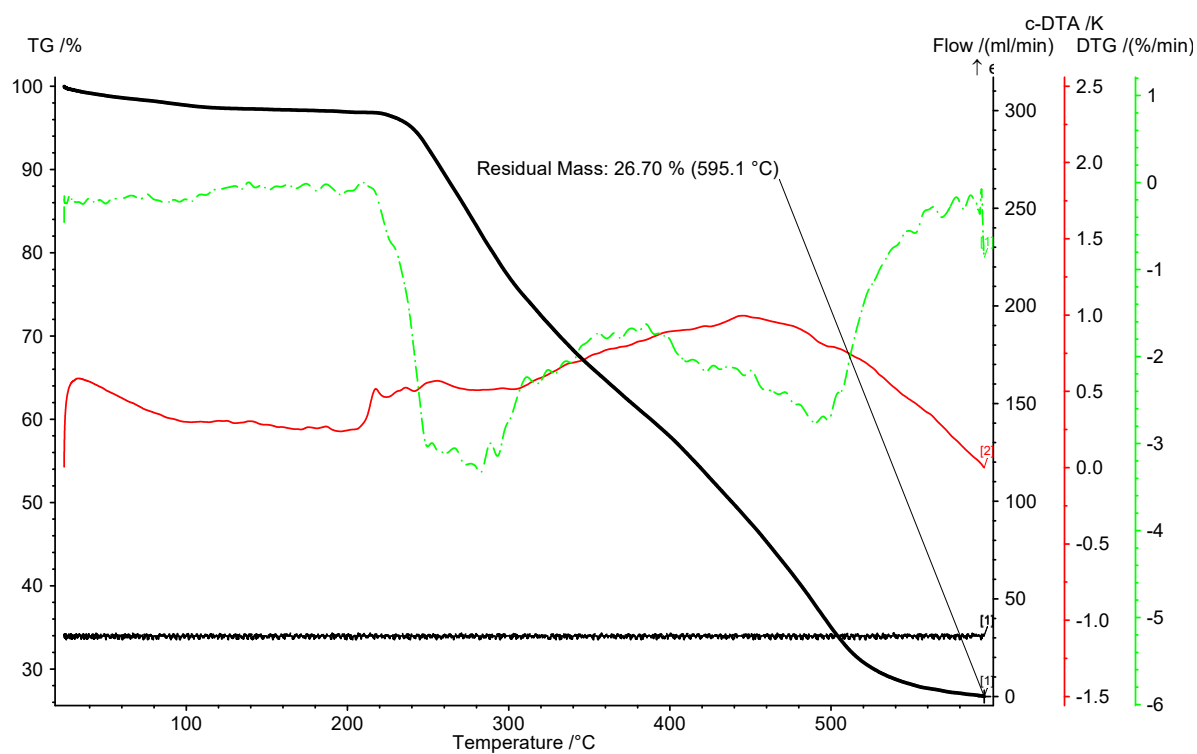
Figure S5. The TGA, DTA & DTG curves for co-crystal **2**.
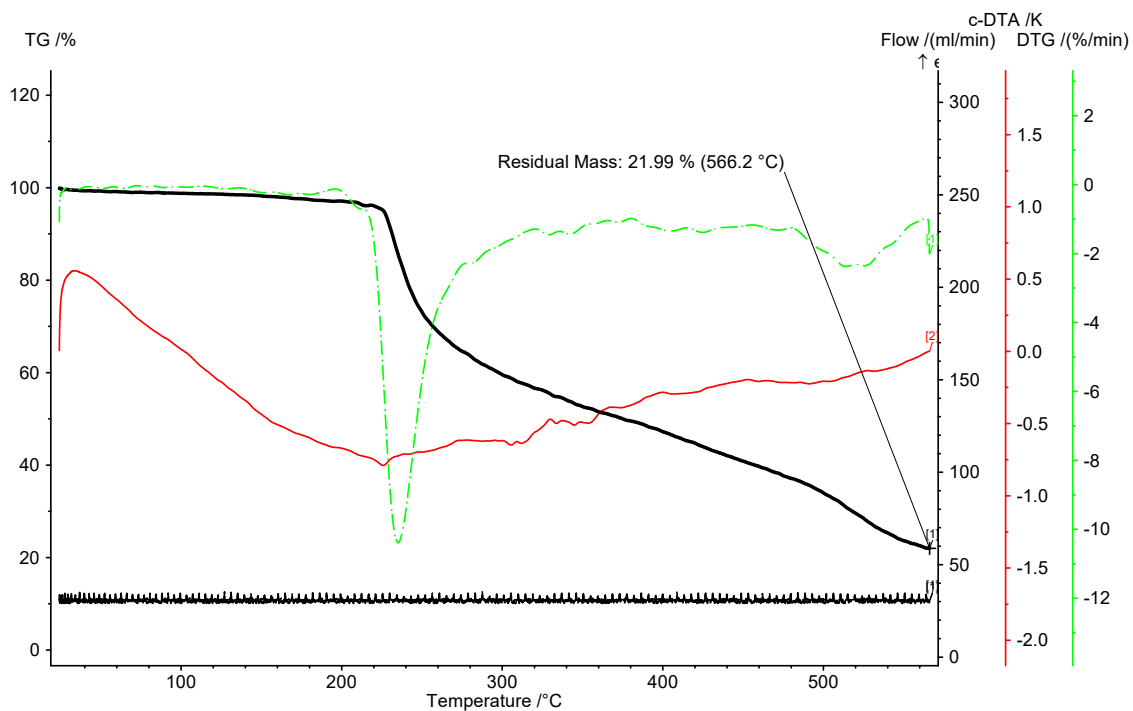
Figure S6. The TGA, DTA & DTG curves for complex **3**.

§3. FT-IR spectra
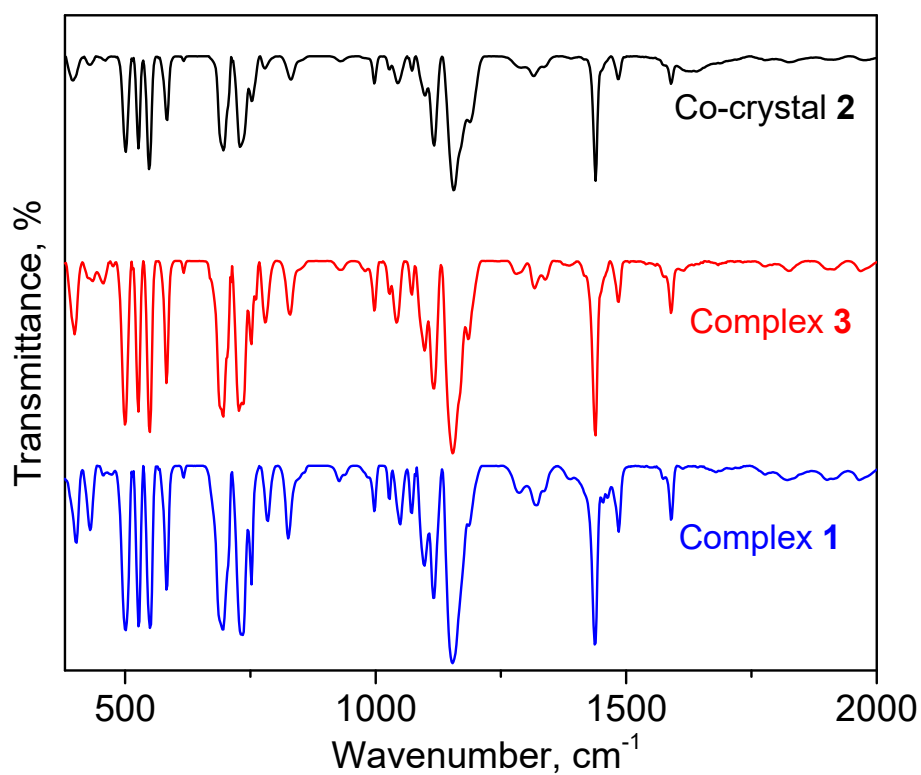
Figure S7. FT-IR spectra of complexes **1**–**3**.

§4. Photophysical study

Corrected photoluminescence spectra were recorded on a Fluorolog 3 spectrometer (Horiba Jobin Yvon) with a cooled PC177CE-010 photon detection module equipped with an R2658 photomultiplier. The luminescence decays were measured on the same instrument. The absolute photoluminescence quantum yields (Φ_{PL}) were determined using a Fluorolog 3 Quanta-phi device. Temperature dependences of luminescence were carried out using Optistat DN optical cryostats (Oxford Instruments).
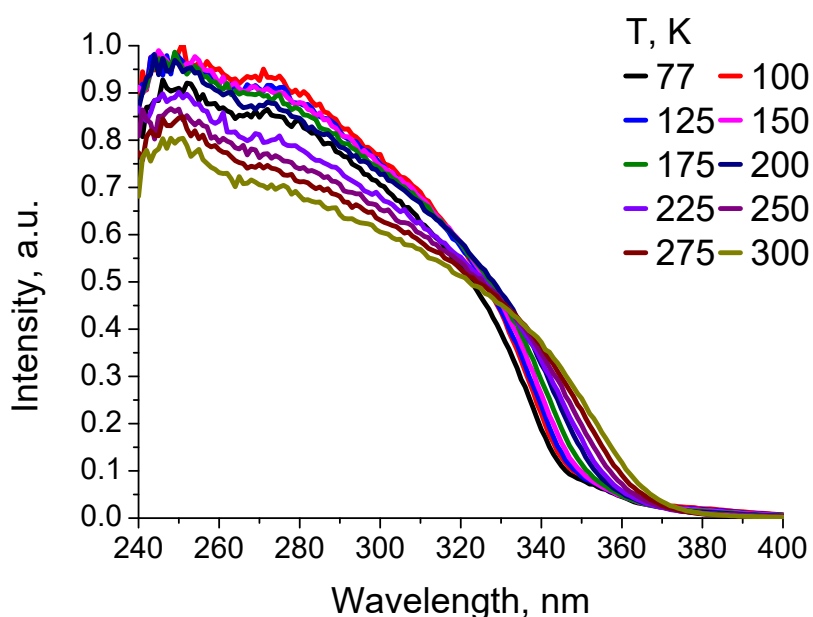
Figure S8. Temperature-dependent excitation spectra of solid ligand **L** recorded at λ_{em} = 410 nm.
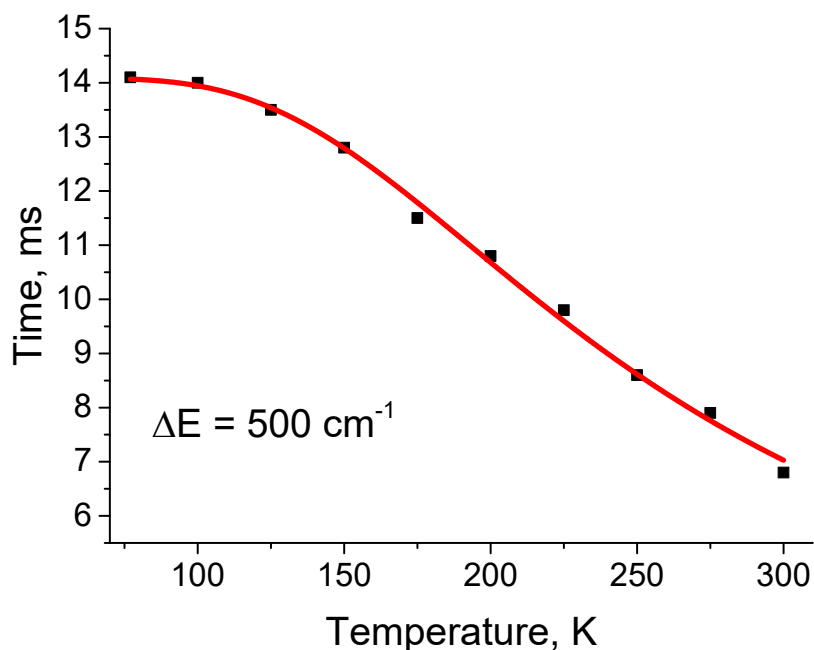
Figure S9. Temperature dependence of the lifetimes of solid **3** (λ_{em} = 630 nm, λ_{ex} = 350 nm). The fitting curve (red line) was plotted using Equation 1 (see in the main text) to the experimental dataset. The resulting fit parameter is ΔE_A = 500 cm^{-1}, representing the activation energy of thermal quenching of photoluminescence of **3**.
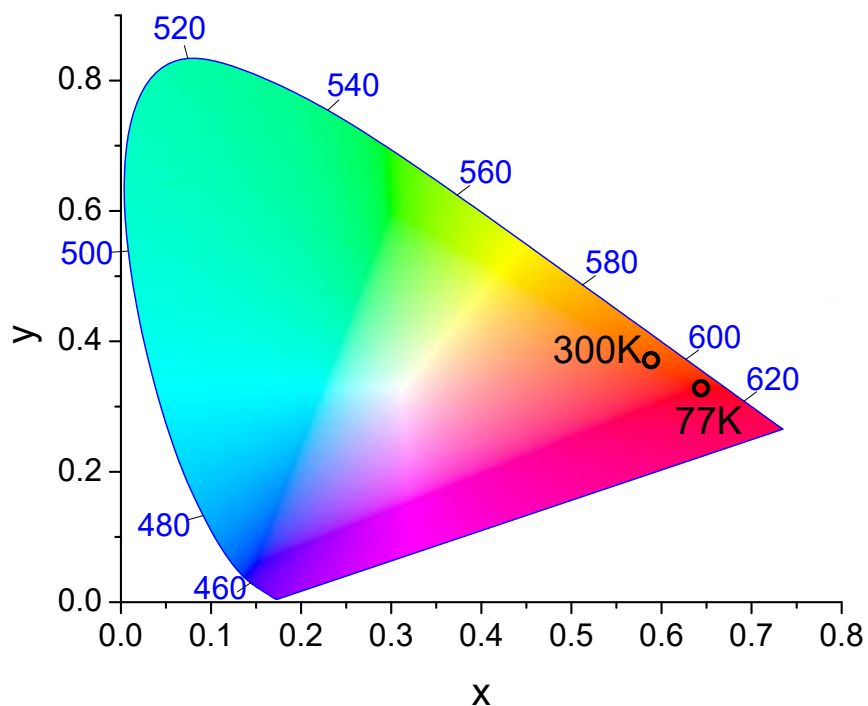
Figure S10. CIE 1931 diagram showing photoluminescence chromaticity for solid **3** at 77 and 300 K (λ_{ex} = 350 nm).
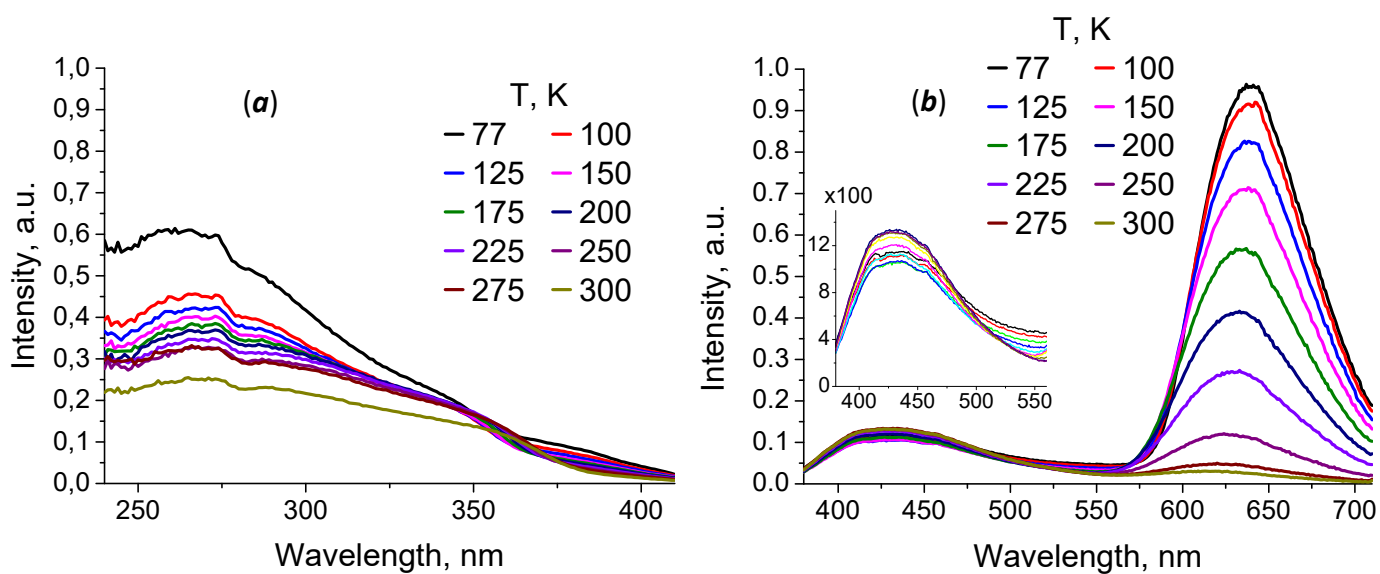
Figure S11. (*a*) Temperature-dependent excitation spectra of solid **2** recorded at λ_{em} = 425 nm; (*b*) Temperature-dependent emission spectra of solid **2** recorded at λ_{ex} = 360 nm.
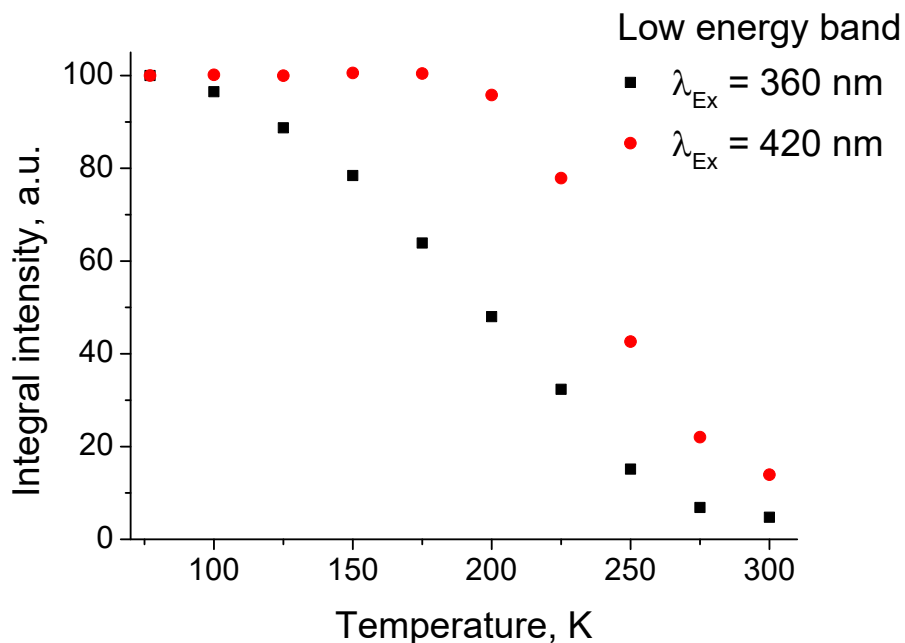
Figure S12. Temperature dependence of integrated emission intensities for LE band (λ_{em} = 640 nm) of **2** at different excitations (λ_{ex} = 360 and 420 nm).
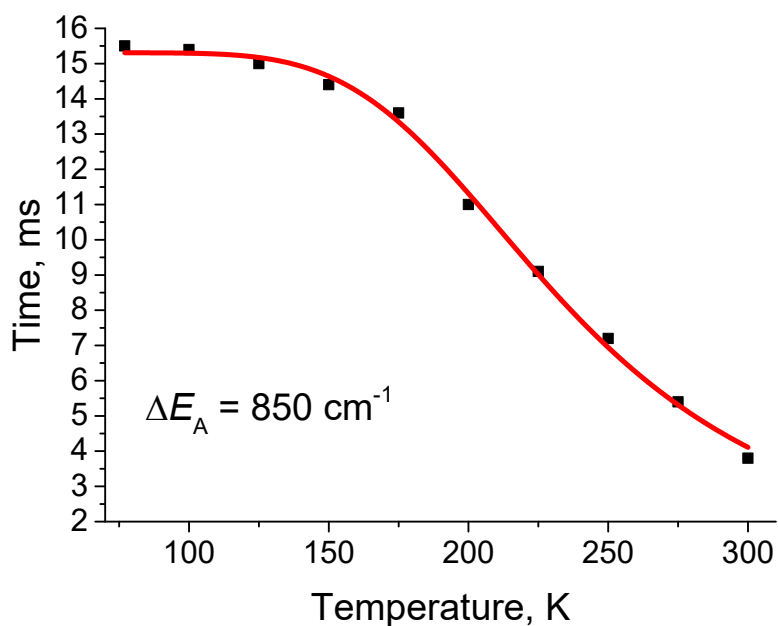
Figure S13. Temperature dependence of the lifetimes of solid **2** (λ_{em} = 640 nm, λ_{ex} = 300 nm). The fitting curve (red line) was plotted using Equation 1 (see in the main text) to the experimental dataset. The resulting fit parameter is ΔE_A = 850 cm^{-1}, representing the activation energy of thermal quenching of photoluminescence of **2**.

§5. Discussion of the symmetry effect on the splitting of the Mn²⁺ terms

To correctly assign the transitions responsible for emission of Mn^{2+} in C_{4v} environment, the effect of symmetry on the degeneracy and splitting of the terms of Mn^{2+} ion has been considered. Octahedral crystal field splits the energy of the 3d ion orbitals into $E(dz^2, dx^2-y^2)$ and $T(dxy, dxz, dyz)$ levels. Removal of one of the apical atoms leads to the formation of the square pyramidal environment (C_{4v} point group) with splitting into $B_1(dx^2-y^2)$, $A_1(dz^2)$, $B_2(dxy)$, $E(dxz, dyz)$ levels. Changing of the crystal field from the octahedral to the square pyramidal leads to the removal of degeneracy and a twice degenerate $E(dxz, dyz)$ state has the lowest energy (**Figure S14**). For the $3d^5$ ion, the energy gaps between the different energy levels are presented in **Table S2**. In the case of the small energy gaps, the Jahn-Teller distortions for the high spin d^5 electron configurations may not occur.
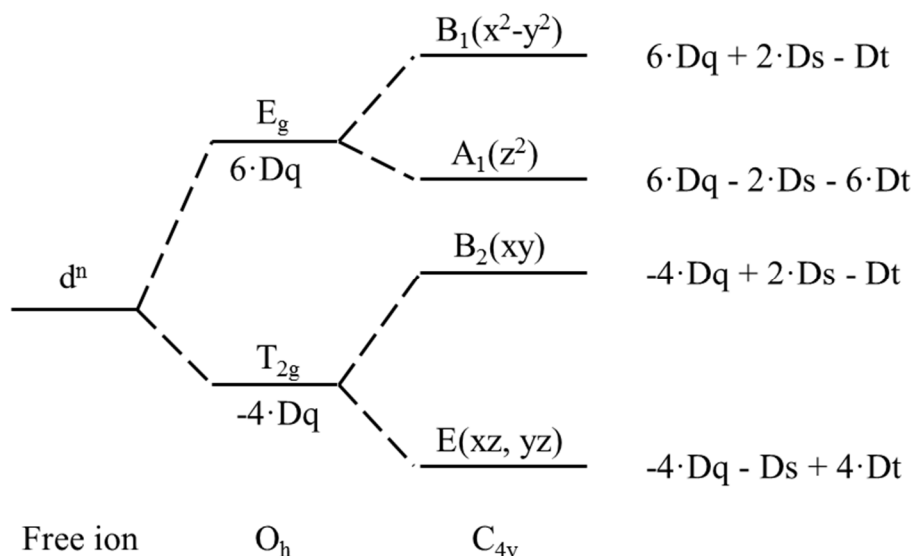
Figure S14. Energy level diagram of the $3d^n$ ion in octahedral and tetragonal fields. Dq is octahedral crystal field and Ds and Dt are tetragonal field parameters. The same sign of Dq and Dt indicates an axial compression and opposite sign indicates an axial elongation.

Table S2. Energy gaps between different energy levels for the $3d^5$ ion.

	Energy gap
E − B₂	-3·Ds + 5·Dt
A₁ − B₁	-4·Ds - 5·Dt
E − A₁	-10·Dq + 1·Ds + 10·Dt
E − B₁	-10·Dq - 3·Ds + 5·Dt
B₂ − A₁	-10·Dq + 4·Ds + 5·Dt
B₂ − B₁	-10·Dq

For C_{4v}, the orbitals are $B_1(dx^2-y^2)$, $A_1(dz^2)$, $B_2(dxy)$, $E(dxz, dyz)$

Table S3. Irreducible representations of the 3d orbitals for different spherical harmonics (the O_h and C_{4v} are considered).

l	O_h	C_{4v}
G	**T₁g**	**E**

	T_{2g}	$B_2 + E$
	E_g	$A_1 + B_1$
	A_{1g}	A_1
D	E_g	$A_1 + B_1$
	T_{2g}	$B_2 + E$
P	T_{1u}	$A_1 + E$
F	A_{2u}	B_2
	T_{1u}	$A_1 + E$
	T_{2u}	$B_1 + E$

For $l = 0$ (**S**) [angular momentum corresponding to the high-spin Mn(II) ion ground state], the irreducible representation of spherical harmonics (multipoles) is A_1 (for both O_h and C_{4v}). Whereas for $l = 4$ (**G**), the terms are $A_{1g} + E_g + T_{1g} + T_{2g}$ for O_h and $2A_1 + A_2 + B_1 + B_2 + 2E$ for C_{4v} (**Table S3**). For $l = 2$ (**D**), there are $E_g + T_{2g}$ for O_h and $A_1 + B_1 + B_2 + E$ for C_{4v}. Lowering of the symmetry from O_h to C_{4v} leads to the splitting of the terms (**Figure S14**). Thus, there are the following absorption (excitation) transitions ${}^6A_1(S) \rightarrow {}^4E(G)$, ${}^4B_2(G)$, ${}^4A_1(G)$, ${}^4B_1(G)$, ${}^4B_2(G)$, ${}^4E(D)$, ${}^4B_2(D)$, ${}^4A_1(D)$, ${}^4B_1(D)$, etc. The $A_1 \rightarrow B_1$ and $A_1 \rightarrow B_2$ transitions are forbidden according to the group theory. Therefore, only $A_1 \rightarrow E$ and $A_1 \rightarrow A_1$ transitions are allowed. Meanwhile, despite such splitting of the energy levels, the emission and excitation spectra of the complexes **1–3** are quite similar to those of the octahedral Mn(II) complexes. It may be caused by the small Ds and Dt tetragonal field parameters. In such a case, the absorption (excitation) spectrum would be close for C_{4v} and O_h. Thus, taking into account the data of **Figure S14** and **Table S3**, it can be assumed that emission of Mn(II) ion with square pyramidal environment is likely originated from the spin-forbidden ${}^4E(G) \rightarrow {}^6A_1(S)$ transition.